



Ultrasound-assisted theophylline polymorphic transformation: Selective polymorph nucleation, molecular mechanism and kinetics analysis

Chen Fang^{a,b}, Peng Yang^{a,b}, Yumin Liu^{a,b}, Jingkang Wang^{a,b}, Zhenguo Gao^{a,b,*}, Junbo Gong^{a,b,*}, Sohrab Rohani^c

^a School of Chemical Engineering and Technology, State Key Laboratory of Chemical Engineering, Tianjin University, Tianjin 300072, China

^b The Co-Innovation Center of Chemistry and Chemical Engineering of Tianjin, Tianjin 300072, China

^c Department of Chemical and Biochemical Engineering, The University of Western Ontario, London, Ontario N6A 5B9, Canada

ARTICLE INFO

Keywords:
Ultrasound
Theophylline
Solute-solvent interaction
Polymorph
Transformation kinetics

ABSTRACT

In this paper, the ultrasound-assisted solvent-mediated polymorphic transformation of theophylline was explored in detail. The induction time and reconstruction time were significantly decreased by ultrasound, thereby decreasing the total transformation time and promoting the transformation process. The ultrasound-promoted efficiency of nucleation was different in three alcoholic solvents, which was difficult to explain by traditional kinetic effects. To resolve the above confusion, binding energies calculated by Density Functional Theory were applied to explore the relationship between the ultrasound-promoted efficiency of nucleation and solute-solvent interactions. Then, a possible molecular self-assembly nucleation pathway affected by ultrasound was proposed: the ultrasound could change and magnify the crucial effect of the specific sites of solute-solvent interactions in the nucleation process. Finally, the transformation kinetics with different effective ultrasonic energies was quantitatively analyzed by Avrami-Erofeev model, indicating that the dissolution element in the rate-limiting step was gradually eliminated by higher ultrasonic energy. Fortunately, the elusive crystal form V could be easily obtained by the ultrasound-assisted polymorph transformation. This proved to be a robust method to produce high purity form V of theophylline. The outcome of this study demonstrated that the proper ultrasonic irradiation had the potential to produce specific polymorphs selectively.

1. Introduction

Polymorphism is the property of a substance to crystallize in different crystalline forms which have different molecular conformation and arrangements in the crystal lattice [1]. Each polymorph of a model compound possesses a unique crystal structure, and consequently reveals different thermodynamic and kinetic properties such as solubility, dissolution rate, stability, and even the mechanical properties like compatibility and tableting [2,3]. According to Ostwald's rule of stages, in the process of solution crystallization, the metastable form crystallizes initially, followed by transformation to the stable crystals at the expense of dissolving metastable crystals [4]. In some cases, the preferential crystallization of stable form or concomitant nucleation of polymorphs (for the condition that both metastable form and stable form simultaneously nucleate) disobey the Ostwald's rule of stages [5,6]. Thus, the production of specific polymorph and the requirements for product

purity often introduce challenges for controlling polymorphs in industry. Due to the requirement of longer storage time, the thermodynamically stable form is usually the preferred form in the pharmaceutical market [7].

The solvent-mediated polymorphic transformation (SMPT) is a popular approach to obtain the more stable polymorph during the process of solution crystallization. This involves two steps: the dissolution of metastable crystals first, followed by the nucleation and growth of stable crystals [8,9]. The SMPT phenomenon has been studied intensively, including the development of monitoring equipment and methods [10,11], the estimation of transformation kinetics [12,13], the effect of solute-solvent interactions on transformation rate [14,15], the transformation intensified by ultrasonic irradiation [16,17], etc. It is well known that the driving force in the SMPT process is the solubility difference between the metastable form and the stable form, but it is not the unique factor to determine the transformation rate. More

* Corresponding authors at: School of Chemical Engineering and Technology, State Key Laboratory of Chemical Engineering, Tianjin University, Tianjin 300072, China.

E-mail addresses: zhenguogao@tju.edu.cn (Z. Gao), junbo.gong@tju.edu.cn (J. Gong).

<https://doi.org/10.1016/j.ultsonch.2021.105675>

Received 1 June 2021; Received in revised form 12 July 2021; Accepted 13 July 2021

Available online 18 July 2021

1350-4177/© 2021 The Authors.

Published by Elsevier B.V. This is an open access article under the CC BY-NC-ND license

(<http://creativecommons.org/licenses/by-nc-nd/4.0/>).

investigations highlight the importance of solute–solvent interaction induced by solvent polarity on the transformation process, and demand a balance between the effect of solubility and solute–solvent hydrogen bond interactions in the transformation process [14,18,19]. In general, the influence of solute–solvent interactions on transformation rate is exhibited in the nucleation and growth of the stable form: (1) the desolvation of solvated solute molecules before forming crystalline nuclei; (2) the removal of solvent molecules from the surface of crystalline nuclei and existing crystals in the slurry [15].

Sonocrystallization is the application of ultrasound to obtain high-value products with desirable characteristics, and the ultrasonic frequency used in sonocrystallization usually ranges from 20 kHz to several MHz. Many studies have reported beneficial results with the assistance of ultrasound in crystallization process, such as promoting nucleation [20,21], narrowing particle size distribution and decreasing agglomeration [22,23], controlling polymorphs [24,25], and accelerating polymorphic transformation [16,26]. Prasad et al. [27] summarized the nucleation mechanism of different polymorphs with the application of ultrasound, and indicated that the ultrasound had the potential to alter the intermolecular interaction of solute. During the studies of ester hydrolysis [28,29], the ultrasonic energy was identified to shift the balance of solvation state by improving the kinetic energy of species, and finally influencing the reaction rate. However, a thorough understanding of the effect of solute–solvent interaction affected by ultrasound on the nucleation process is still unclear, which needs attention. Besides, in our previous study, the ultrasound could change the kinetic mechanism of a transformation system from nucleation-growth control to the growth control [26].

Theophylline is a methylxanthine derivative, and is usually used for treating asthma and chronic obstructive pulmonary disease [30]. Seven anhydrous polymorphs have been reported [30–33], among which form I, II, and V are target polymorphs in this study. Form I and form II are enantiotropically related, and form I is identified to be the stable polymorph above 232 °C, while, form II is more stable at room temperature [34]. Form V crystal is elusive, and for the first time, Roy et al. obtained form V crystals using the technique of CO₂ supercritical antisolvent precipitation at high pressure [30]. Subsequently, minor form V crystals concomitant with amounts of form II crystals were produced by crystallization in methanol [35].

In this work, the SMPT of theophylline (from form I to form II) was studied with the assistance of ultrasound. Three alcoholic solvents and three ultrasonic modes were selected in the experiments. The transformation time was divided into two parts for further analyzing the ultrasound-promoted efficiency: the induction time and reconstruction time of the stable crystal. Little is known concerning the reason that the nucleation-promoted efficiency by ultrasound was different in various solvents. We attempt to make a connection between the ultrasound-promoted efficiency of nucleation and solute–solvent interaction to resolve the confusion. The Density Functional Theory (DFT) was applied to calculate binding energies for probing solute–solvent interactions. A possible molecular self-assembly nucleation pathway affected by ultrasound was proposed to explain the effect of solute–solvent interaction affected by ultrasound on the nucleation process. Then, the transformation kinetics were estimated by the Avrami-Erofeev model to demonstrate the change of transformation rate-limiting step with the application of ultrasound. In addition, it was the first time to utilize the ultrasound to crystallize theophylline form V crystals in the solution at atmospheric pressure. Large amounts of theophylline form V crystals were surprisingly produced during ultrasound-assisted polymorphic transformation process. By this method, highly pure form V crystals could be obtained in 2-propanol, which makes the preparation of this elusive form V of theophylline more accessible.

2. Materials and methods

2.1. Materials

Theophylline was purchased from Shanghai Aladdin Chemistry Co. Ltd. of China with a mass fraction purity larger than 99%, and used without further purification. The theophylline raw materials were the crystals of relatively stable form II, which could not be used for solvent-mediated polymorphic transformation experiments directly. Thus, the metastable form I crystals were prepared by heating the raw materials in a quartz tube furnace (OTF-1200X, HF-Kejing, China) under the protection of circulating nitrogen, at the temperature of 543.15 K for 2 h [31]. Analytical-grade 2-propanol (99.5%) and 1-butanol (99%) were supplied by Shanghai Aladdin Chemistry Co. Ltd. of China. Analytical-grade 1-propanol (99%) was supplied by Shanghai Macklin Biochemical Co. Ltd. of China.

2.2. Ultrasonic processor

The ultrasonic frequency was fixed at 20 kHz using an ultrasonic processor (JY92-IIDN, Scientz, China) providing a maximum irradiation power of 600 W. The tip diameter of the horn was 6 mm, and the immersion depth of the tip in the solution was 1.5 cm providing a direct irradiation mode. To avoid the thermal effect given by ultrasonic irradiation and make the results more reliable, the pulsed ultrasound was chosen for the whole transformation experiments. The experimental group designated as Exp. 1 in Table 1 was conducted without ultrasound. Three ultrasonic modes were applied in the experiments denoted as Exp. 2, 3 and 4, respectively, as shown in Table 1.

2.3. Solubility measurements

The dynamic method was used to measure the solubility of theophylline, which has been proved to be accurate and reliable in published literatures [36,37]. The experimental equipment was similar to that using laser monitoring method in many published literatures [38,39]. The detailed measurement method could be found in the Supporting Information. The solubility of form I and form II of theophylline at two temperatures in different solvents is listed in Table 2.

2.4. Ultrasound-assisted solvent-mediated polymorphic transformation

The SMPT process should be implemented in the saturated solution of metastable crystals. Then, certain amounts of metastable crystals are suspended in this saturated solution to form the suspended solution (turbid solution). The whole system undergoes the dissolution of metastable crystals and the crystallization of stable crystals, until all of the metastable crystals transform to the stable crystals, indicating that the polymorphic transformation process has been completed [8,9]. Based on the above principle, the SMPT process of theophylline was investigated in 1-propanol, 2-propanol and 1-butanol. Based on the solubility of theophylline form I at 303.15 K, a certain amount of form I crystal was added to a crystallizer with 50 g solvent to prepare the saturated solution. To conduct the whole transformation process at a constant temperature (303.15 K), a thermostatic water bath (CF41, Julabo, Germany) was employed. Furthermore, the solute and solvent

Table 1
The ultrasonic operating parameters used in polymorphic transformation experiments.

Exp.	Frequency (kHz)	Rate Power (W)	Duty cycle
1	0	0	None
2	20	6	2 s ON and 15 s OFF (11.76%)
3	20	6	2 s ON and 2 s OFF (50%)
4	20	60	2 s ON and 2 s OFF (50%)

Table 2
The solubility of theophylline in three solvents at different temperatures.

solvent	Temperature T (K)	Form I Solubility c_1^* (mg/g solvent)	Form II Solubility c_2^* (mg/g solvent)	Δc (mg/g solvent)
1-propanol	303.15	4.53 ± 0.17	4.08 ± 0.08	0.45
	308.15	5 ± 0.12	4.32 ± 0.13	0.68
2-propanol	303.15	2.32 ± 0.09	1.98 ± 0.13	0.34
	308.15	3.36 ± 0.10	2.83 ± 0.10	0.53
1-butanol	303.15	3.82 ± 0.11	3.56 ± 0.12	0.26
	308.15	4.62 ± 0.07	4.18 ± 0.10	0.44

c_1^* , c_2^* : solubility of form I and form II crystals, which also represent for the saturated solution concentrations.
 Δc : the solubility difference between form I and form II.

were intensively mixed with a magnetic stirrer (ZNCL-BS, Xingke Sci. Ltd., China) at 300 rpm (about 30 min) to obtain a homogeneous saturated solution. Then, 1 g form I crystals were added to the above homogeneous saturated solution to obtain a turbid solution which was used to study the transformation process. The turbid solution was stirred at 300 rpm for transformation in the absence and presence of ultrasound at 303.15 K. For Exp. 2–4, pulsed ultrasonic irradiation was introduced into the turbid solution until form I crystals completely transformed to form II crystals. To illustrate the effect of ultrasound on the transformation process at different temperatures, the transformation experiments with and without ultrasound at 308.15 K were also investigated following the same operating steps as those used at 303.15 K.

It should be noted that 1 g suspended solid applied in this study was determined by lots of pre-experiments, keeping the transformation time within proper bounds (about 8–18 h at the condition without ultrasound). With 1 g suspended solid, the effect of ultrasound was obvious enough and could be distinguishable in these organic solvents. Besides, to reduce the interference of secondary nucleation, we did not add form II crystals as seeds in the whole transformation experiments.

The polymorphic composition in the transformation process was monitored by *in-situ* Raman spectroscopy (ReactRaman 785, Mettler-Toledo, Switzerland). UV–vis spectroscopy (UV-3010 spectrophotometer, Tokyo, Japan) was used to determine the real-time theophylline concentration in the solution during the transformation process. Before extracting the liquid samples, the stirring and ultrasonic irradiation were stopped for 3 min to obtain supernatant liquid. Several liquid samples (about 6–8 samples, each 0.5 ml) were pipetted out at certain time intervals. The liquid sample was filtered through a preheated 0.22 μm syringe filter and further diluted to measure the peak intensity at 270 nm. The standard curve ($R^2 = 0.999$) was plotted using five samples of known theophylline concentration. To calculate the transformation kinetic parameters, the quantitative analysis of the polymorphic composition was determined by powder X-ray diffraction (PXRD, Rigaku D/MAX 2500 X-ray diffractometer (Rigaku, Japan) at 40 kV and 100 mA with Cu-K α radiation ($\lambda = 1.54178 \text{ \AA}$)). Six samples were extracted at certain time intervals during the transformation process, and the dried solid samples were obtained through vacuum filtration, which could be used for the polymorphic composition measurement.

3. Results and discussion

3.1. Monitoring results of ultrasound-assisted theophylline transformation

The two model compounds of theophylline (form I crystals and form II crystals) could be distinguished by Raman spectra. The Raman spectra of theophylline in solid state and solution state were respectively shown in Fig. 1. The spectra in Fig. 1(a) expressed distinct differences between the two forms, which could be used as indicators for *in-situ* tracking form I and form II crystals. The metastable form I has characteristic peaks at 1331 and 1400 cm^{-1} , whereas the stable form II has characteristic peaks at 1315, 1426 and 1665 cm^{-1} . Based on the reported literatures [40–42], the key bands at 1331 and 1400 cm^{-1} represent the –CN stretching on the imidazole ring, the key band at 1315 cm^{-1} belongs to

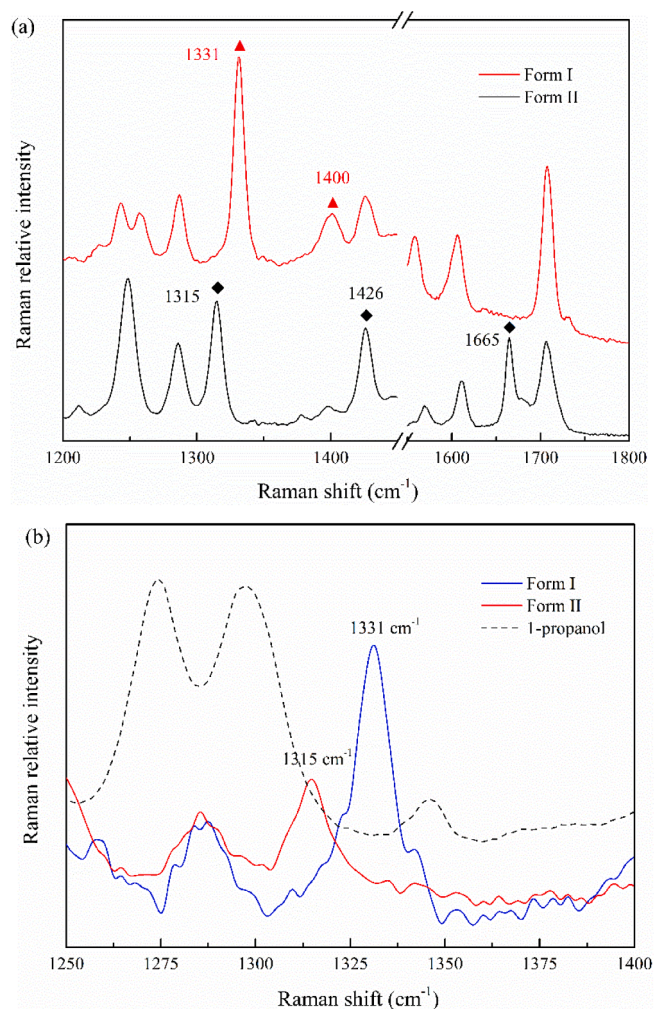


Fig. 1. (a) Solid-state Raman spectra: the solid triangles and solid diamonds represent the main characteristic peaks for form I crystals and form II crystals, respectively; (b) One segment of Raman spectra in solution (1250–1400 cm^{-1}): form I and form II crystals in 1-propanol suspension.

the stretching of imidazole ring, the key band at 1426 cm^{-1} corresponds to the –CH₃ in-plane deformation of pyrimidine ring, and the key band at 1664 cm^{-1} can be assigned to the C = O stretching on the pyrimidine ring. To track the whole transformation process, the characteristic peak intensity of the model compound should be clear and distinguishable in the organic solvent suspension, so that the solvent spectra could be deducted to reduce the disturbance. Fig. 1(b) depicted the characteristic peaks of two form crystals (1331 cm^{-1} for form I, and 1315 cm^{-1} for form II) in the 1-propanol suspension, in which the solvent spectrum has been deducted. The same operation was also applied in 2-propanol and

1-butanol suspension, and the characteristic peaks position of the two form crystals did not change. Therefore, the peaks at 1315 and 1330 cm^{-1} can be used for real-time determination of the solid content variation in the transformation process.

To illustrate the monitoring situation, the Raman relative intensity variations with time were shown in Fig. 2. Along with the transformation process, the Raman relative intensity of form I (1331 cm^{-1}) decreases and the intensity of form II (1315 cm^{-1}) increases, following the directions of the arrows. The location and intensity changes of characteristic peaks in 2-propanol and 1-butanol were depicted in Fig. S1, and showed a similar variation trend to that in 1-propanol.

To verify the enhancement of transformation by ultrasonic irradiation and clarify the effect of ultrasonic irradiation on the transformation kinetics, the process in multiple ultrasonic modes should be analyzed seriously. As depicted in Fig. 3, various ultrasonic modes were applied to the theophylline transformation experiments in the 1-propanol solution (at 303.15 K), and the transformation processes were intensely accelerated by ultrasound. As described in the introduction section, it is suggested that the solvent-mediated transformation process of theophylline polymorphs involves two consecutive steps: the dissolution of metastable form I crystals, the nucleation and growth of the stable form II crystals. As shown in Fig. 3, there is a time period before the nucleation of stable crystals in all four experiments, namely a plateau exists before the decline of peak intensity at 1331 cm^{-1} or the increase of peak intensity at 1315 cm^{-1} . To investigate the transformation process quantitatively, the total transformation time (t_{total}) was divided into two parts, one was considered as the induction time (t_{ind}) and the other one was counted as the reconstruction time (t_r) [43–45]. The induction time, t_{ind} , is the time period from the initiation of the phase transformation to the first nucleation of stable crystals, and the reconstruction time, t_r , is the time period beginning from the end point of induction time to the time point that all the metastable crystals have been converted to the stable crystals [32,46].

The specific time periods were marked and indicated in Fig. 3(a). Without ultrasound (Fig. 3(a)), the experiment required about 576 min to complete the transformation process. To highlight the intensifying effect of ultrasound, three different modes of pulsed ultrasound were applied to the transformation process. A slightly lower power of 6 W with the duty cycle of 11.76% could sharply shorten the total transformation time to 355 min, as shown in Fig. 3(b). The significant improvement of transformation efficiency by the weak ultrasonic energy could improve process efficiency. Then fixing the rate power and increasing the duty cycle to 50%, shown in Fig. 3(c), the total

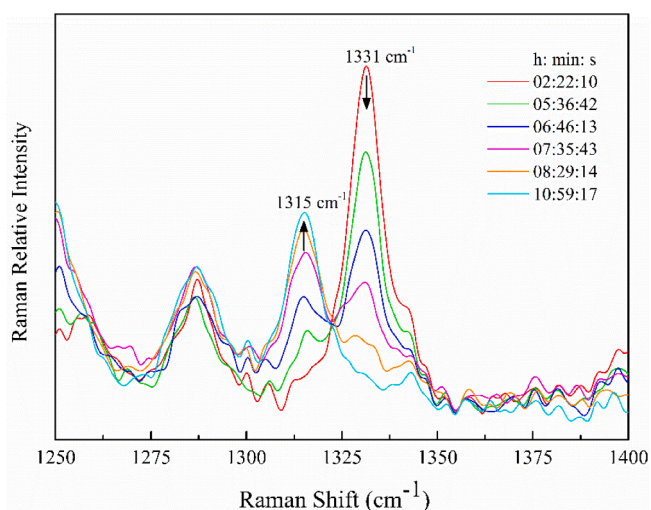


Fig. 2. The variations of *in-situ* Raman characteristic peaks intensity with time in the 1-propanol mediated transformation process at 303.15 K without ultrasound.

transformation time was decreased to 165 min. The longer the effective ultrasonic irradiation worked, the shorter the transformation time needed. Finally, keeping the duty cycle at 50%, the rate power was increased to 60 W. As shown in Fig. 3(d), the total transformation time was about 150 min, only a slight decrease (15 min) compared to the t_{total} in Fig. 3(c). It indicates that the active effect of ultrasound on the theophylline transformation process is limited. The upper limit of the effect may be attributed to the influence of ultrasound on the transformation kinetics.

According to the studies on polymorph transformation kinetics, the rate-limiting step could be identified by the real-time relative change of solid-state composition and solution concentration [47–49]. Especially, the variation of Raman peak relative intensity could represent the change of solid-state composition [50,51]. In Fig. 3(a), without ultrasound (Exp.1), the solution concentration was kept at a plateau corresponding to the solubility of metastable form I, before the nucleation of stable form II started. Then, with the solution concentration slowly decreasing to the solubility of stable form, the metastable crystals in the solid-state composition almost disappeared. The scenario in Exp. 1 seemed to be close to the nucleation-dissolution controlled polymorph transformation [47,48]. However, a subtle difference existed during the period from the onset of decline in the solution concentration to reaching the solubility of the stable form. The decline of solution concentration is quite fast in the nucleation-dissolution controlled polymorphic transformation. The solution concentration decreases to the solubility of the stable form before the disappearance of metastable crystals in the solid-state composition. Thirunahari [49] demonstrated that the rate-limiting step for the transformation process (similar to Fig. 3(a)) was the primary nucleation of the stable form, and the dissolution of metastable crystals and growth of stable crystals were equally fast. In the presence of ultrasound, the plateau period of solution concentration began to exceed the plateau period (t_{ind}) of solid content. This is shown in Fig. 3(c) and Fig. 3(d). The rate-limiting steps in Fig. 3(c) and Fig. 3(d) were close to the nucleation-growth controlled polymorph transformation. As a result, the ultrasound could change the kinetics of solvent-mediated polymorphic transformation. The rate-limiting step during theophylline transformation process, in this study, changed gradually from nucleation-limiting to nucleation-growth-limiting. Namely, the ultrasound controlled the rate-limiting step in the transformation process by changing the competitive relationship among dissolution rate, nucleation rate and growth rate.

Fig. 4 summarized the t_{total} , t_{ind} and t_r during the theophylline transformation process in three alcoholic solvents at 303.15 K, which could provide a better comparison for the theophylline transformation process in these solvents. It was obvious that the order of the total transformation time, t_{total} , in these alcoholic solvents was 1-butanol > 2-propanol > 1-propanol (meaning that transformation rate: 1-propanol > 2-propanol > 1-butanol). In the absence of ultrasonic irradiation (Exp. 1), the t_r presented the same order with t_{total} , while the order of t_{ind} in these solvents was 2-propanol > 1-butanol > 1-propanol. According to the reported studies, the rate of solvent-mediated polymorphic transformation depends on three key factors: (1) the solute solubility in the solvent [51,9]; (2) the solubility difference between the metastable and stable crystals [8,52]; and (3) the interaction between the solute and solvent molecules [14,15]. Accordingly, the transformation process tends to be influenced by two or all of the above factors.

Increasing the solute solubility would accelerate the rate of transformation to the stable form [51,9]. The order of the theophylline solubility (in Table 2) was 1-propanol > 1-butanol > 2-propanol, which did not match the order of transformation rate. However, Δc , the solubility difference between the metastable and stable crystals in Table 2, had the same order as the transformation rate in Exp. 1. Many studies pointed out that the solubility difference between the metastable form and stable form was usually used as the supersaturation for studying the polymorphic transformation process [15,18,32]. A larger solubility difference provided a faster mass transfer rate not only for the dissolution but

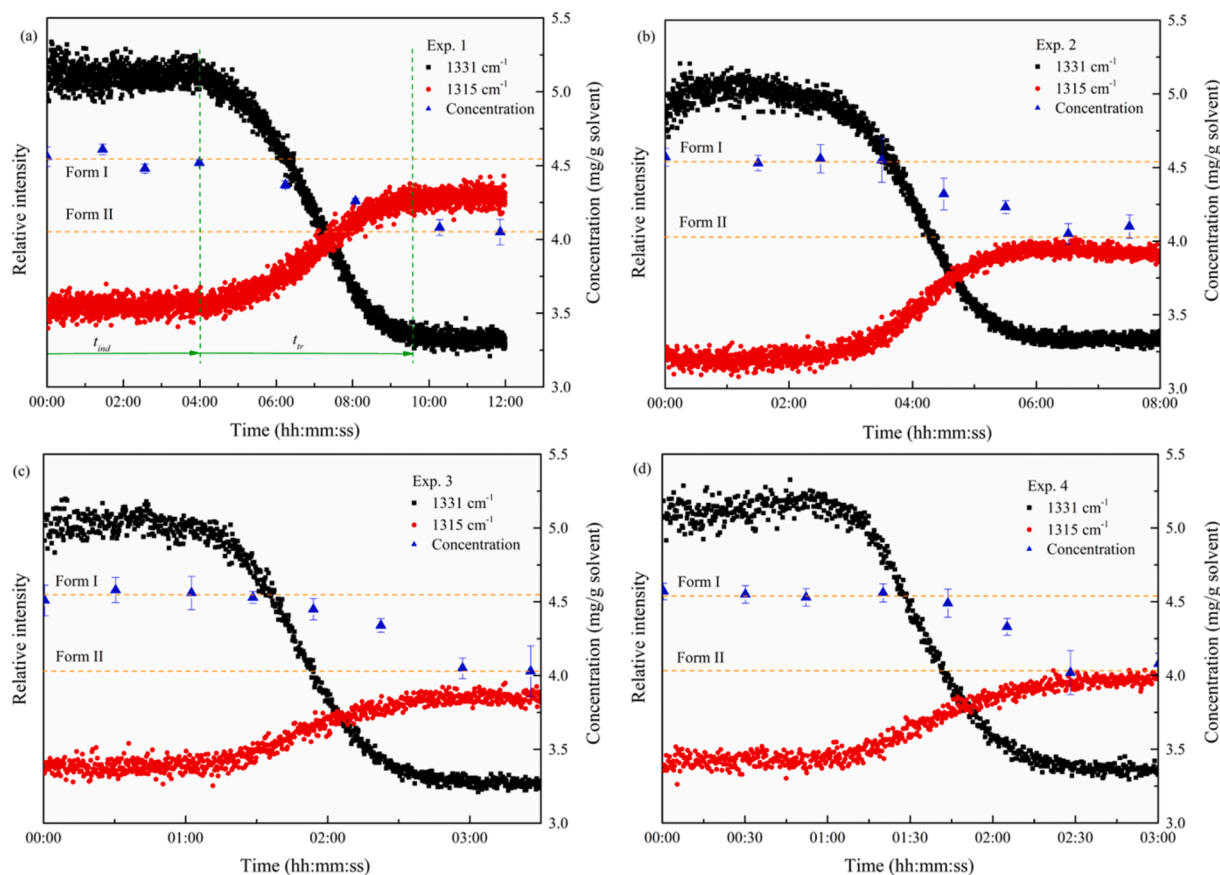


Fig. 3. The variations of Raman relative intensity and solution concentration in the transformation process from form I to form II crystals in 1-propanol suspension with different ultrasonic modes (described in Section 2.2): (a) Exp. 1; (b) Exp. 2; (c) Exp. 3; (d) Exp. 4.

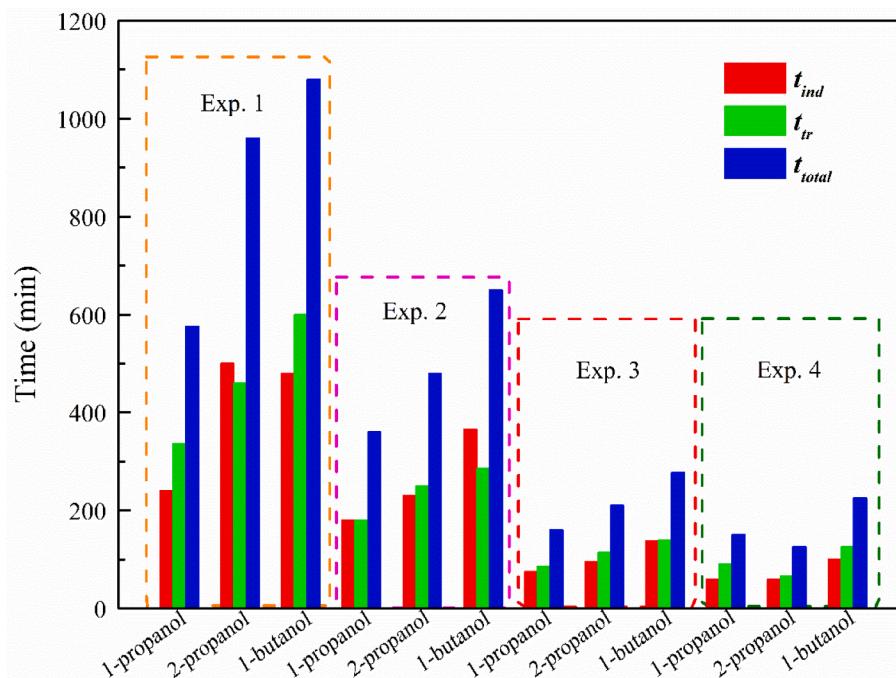


Fig. 4. The distribution of t_{ind} , t_{tr} and t_{total} in the theophylline transformation process of Exp.1-4 at 303.15 K.

also for the crystal nucleation and growth in the transformation process [8]. Thus, the rate of transforming from theophylline form I to form II was constrained by Δc which acted as the driving force. Finally, the

theophylline and solvent molecular interaction would influence the nucleation and growth of the stable crystals, which also influenced the subsequent transformation. The specific description was listed in Section

3.3.2. In the presence of ultrasonic irradiation (from Exp. 2 to Exp. 4), all these three time periods were shortened. Though with the weakest effective ultrasonic irradiation in Exp. 2, these three time periods revealed a trend of sharp decrease, comparing with the results without ultrasound (Exp. 1). In particular, the order of t_{ind} (in Exp. 2) in these solvents began to change: 1-butanol > 2-propanol > 1-propanol. But, the order of t_{tr} and t_{total} in Exp. 2 still conformed with that in Exp.1. Then, comparing the results in Exp. 2 (duty cycle: 11.76%) with that in Exp. 3 (duty cycle: 50%), the longer the effective ultrasonic irradiation worked, the shorter t_{total} needed, and so did t_{ind} and t_{tr} . The order of t_{ind} , t_{tr} and t_{total} in Exp. 3 is consistent with that in Exp. 2. Higher ultrasound power would provide stronger cavitation effect, which had a direct influence on the nucleation and mass transfer. Accordingly, t_{ind} , t_{tr} and t_{total} were further shortened in Exp. 4 (60 W) than in Exp. 3 (6 W). But owing to the limitation of transformation kinetic, the extent of decrease was minor. It seemed that the effect of ultrasound on this system has been reached its upper limit with the condition in Exp. 4.

The distribution of t_{ind} , t_{tr} and t_{total} in the theophylline transformation process at 308.15 K was shown in Fig. S2, and the effect was similar to that at 303.15 K. Besides, with higher transformation temperature, the shorter was the total transformation time, including the nucleation period and reconstruction period of stable crystals. The higher temperature increased solubility difference, which accelerated the rate of dissolution, nucleation and crystal growth in phase transformation, and accordingly produced a faster transformation process. It was expected that the ultrasound could facilitate the phase transformation, especially in shortening the nucleation period [16,17,26]. It can be seen from Exp. 4 in Fig. 4 and Fig. S2, that the order of t_{ind} follows 1-butanol > 2-propanol \approx 1-propanol, and the order of t_{total} was 1-butanol > 1-propanol \geq 2-propanol. These trends seem to be different from those observed in the absence of ultrasound in Exp. 1. Evidently, the degree of time reduction was different in these solvents. In other words, it was obvious that the efficiency of ultrasound on the theophylline transformation process was different in these alcoholic solvents.

3.2. The variation of ultrasound-promoted efficiency in different solvents

To find out the reason for the difference in ultrasound-promoted efficiency (E), the decrease in t_{ind} , t_{tr} and t_{total} was calculated and listed in Table 3. Table 3 summarized the t_{ind} , t_{tr} , t_{total} and E for the solvent-mediated polymorphic transformation in Exp. 1 and Exp. 4. The ultrasound-promoted efficiency is defined in Eq. (1), in which t_i^1 and t_i^4 represent the time in Exp. 1 and Exp. 4. t_i represents t_{ind} , t_{tr} and t_{total} in each experiment.

$$E = \frac{t_i^1 - t_i^4}{t_i^1} \times 100\% \quad (1)$$

In Table 3, at 303.15 K, the t_{ind} without ultrasound (Exp. 1) for 1-propanol, 2-propanol and 1-butanol, were 240 s, 500 s and 480 s. In Exp. 4, these periods decreased to 60 s, 60 s and 100 s, respectively, with 60 W ultrasound. Generally, the nucleation rate is considered to be inversely proportional to the induction time [7,8,45].

In this work, the nucleation-promoted efficiency by ultrasound was reflected by the decrease in t_{ind} . At 303.15 K, the nucleation rate in Exp.

4 (with 60 W ultrasound) was the highest in 1-propanol and 2-propanol, follow by 1-butanol, which was different from the order of nucleation rate without ultrasound (1-propanol > 1-butanol > 2-propanol in Exp. 1). The ultrasound-promoted efficiency of t_{ind} was analyzed and followed the order of 2-propanol (88.00%) > 1-butanol (79.17%) > 1-propanol (75.00%) with 60 W ultrasound (Exp. 4). This indicated that the ultrasound had the largest promoting effect on nucleation rate in 2-propanol, then in the 1-butanol, and last in 1-propanol. It is well known that ultrasound could promote crystal nucleation, and accelerate nucleation rate. At first, we speculated that the ultrasound-promoted efficiency would be larger for an easier nucleation system, or even for an easier transformation system. But the results in this study demonstrated a conflicting conclusion. The nucleation rate order without ultrasound at 308.15 K was consistent with that at 303.15 K. However, the ultrasound-promoted efficiency order of t_{ind} at 308.15 K followed by 2-propanol (86.67%) > 1-propanol (77.50%) > 1-butanol (76.92%). It demonstrated that the ultrasound had the largest promoting effect on nucleation rate in 2-propanol, then in the 1-propanol, and last in 1-butanol.

Similarly, the growth-promoted efficiency and transformation-promoted efficiency by ultrasound could be reflected by decreasing degrees in t_{tr} and t_{total} , respectively. At 303.15 K, the ultrasound-promoted efficiency (60 W) on t_{tr} and t_{total} followed the decreasing sequence by 2-propanol, 1-butanol and 1-propanol. While, at 308.15 K, the ultrasound-promoted efficiency (60 W) on t_{tr} and t_{total} followed by 2-propanol > 1-propanol > 1-butanol.

To the best of authors' knowledge there is no relevant studies to investigate the reason why ultrasound could have different enhancement efficiencies on the nucleation rate in different solvents. In addition, no reason has been presented for different ultrasound enhancement efficiencies on the growth rate and transformation rate in different solvents. Secondary nucleation and fragmentation of stable crystals may counteract the crystal growth of stable crystals during the reconstruction process in the presence of ultrasound [53–56]. Thus, it is difficult to comprehensively explore the reason for the differences in the enhancement efficiency of crystal growth rate by ultrasound in various solvents. Both the ultrasound-promoted efficiency on the nucleation stage and reconstruction stage determined the ultrasound-promoted efficiency on the whole transformation process in different solvents. The reason for the various effects of ultrasound on nucleation rate in different solvents is discussed below.

3.3. Molecular mechanism in the nucleation stage

3.3.1. Crystallization of the form V crystals of theophylline with ultrasound

To resolve the above confusion, PXRD was used to identify the theophylline polymorphs during the transformation process. Fig. S3 showed the PXRD patterns of metastable form I and stable form II. The main characteristic peaks located at 11.2°, 13.5° and 14.6° represent the metastable form I, and the main characteristic peaks located at 7.1°, 12.6° and 25.5° represent the stable form II. The microscope images of the two polymorphs were shown in Fig. S4 for the morphology comparison. Fig. S4(a) presented that form I crystals were needle-like with larger aspect ratio, and Fig. S4(c) presented that form II crystals were

Table 3

The summary of t_{ind} , t_{tr} , t_{total} and E in three solvents at different temperatures.

Temperature (K)	Time (min)	Exp. 1			Exp. 4			Efficiency (E)		
		t_{ind}	t_{tr}	t_{total}	t_{ind}	t_{tr}	t_{total}	t_{ind}	t_{tr}	t_{total}
303.15	1-propanol	240	336	576	60	90	150	75.00%	73.21%	73.96%
	2-propanol	500	460	960	60	66	126	88.00%	85.65%	86.88%
	1-butanol	480	600	1080	100	125	225	79.17%	79.17%	79.17%
308.15	1-propanol	200	294	494	45	63	108	77.50%	78.57%	78.14%
	2-propanol	360	320	680	48	66	114	86.67%	79.00%	83.24%
	1-butanol	325	430	755	75	120	195	76.92%	72.09%	74.17%

plate-like with damaged edges. With the same magnification, form II crystals were much smaller than form I crystals, as shown in Fig. S4(b). Both of the two polymorphs were thin and fragile crystals, and the fragments of the two polymorphs were difficult to distinguish by the morphology. Thus, microscope images could act as an auxiliary means for identifying the polymorphs in theophylline transformation.

Without the ultrasound, the transformation products were pure form II crystals, which was presented in Fig. S5. However, a unique PXRD pattern, different from form I and form II, appeared with 60 W ultrasound, as shown in Fig. 5. Comparing with the X-ray diffraction pattern of form V provided by the Roy [30], the PXRD pattern in Fig. 5 (3) has the same characteristic peaks at 6.8°, 12.9° and 13.6°. Thus, the obtained unique crystals could be confirmed to be theophylline form V. The products in Fig. 5 (3) were almost pure form V, obtained by transformation of form I crystals in 2-propanol with 60 W ultrasound at 308.15 K. In addition, form V crystals also could be obtained by the transformation in other solvents, such as in 1-butanol with 60 W ultrasound at 308.15 K (Fig. 5 (4)). The PXRD pattern in Fig. 5(4) included characteristic peaks of both form V and form II, which indicated that a mixture of form V and form II crystals were obtained in transformation products.

During the transformation process, the intermittent sampling results identified the relative stability of the above polymorphs (Fig. S6). First, form II and form V crystals appeared simultaneously after the induction time. Then, form V crystals disappeared with time and finally only form II crystals remained in the solution. As a result, form II is the stable crystal form, while form I and form V are metastable forms. The relative stability of these three polymorphs follows form I < form V < form II in the experimental condition. Form II and form V could also be distinguished by Raman spectra, as shown in Fig. S7. Characteristic peaks after 300 cm⁻¹ were almost at the same position for form II and form V. There is an obvious difference between the two form crystals at about 200 cm⁻¹, with form II at 211 cm⁻¹ and form V at 228 cm⁻¹. Unfortunately, the peaks at these wavelengths were too weak in the solvent to monitor the transformation process accurately by in-situ Raman tracking.

In order to analyze the polymorphic nucleation behavior after the induction time, polymorphs nucleated by transformation were monitored and summarized in Fig. 6. The samples were collected from the reconstruction zone and analyzed for PXRD testing (Fig. S8).

Combining Fig. 6 with Fig. S8(a), only form II crystals were

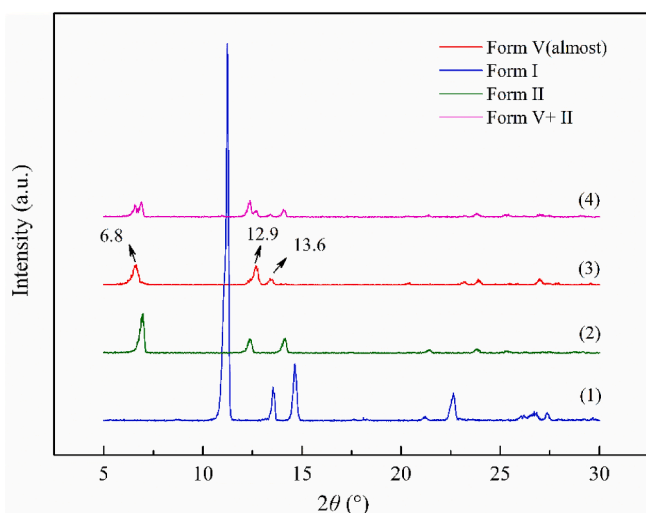


Fig. 5. PXRD patterns of theophylline form I, form II and form V: (1) form I, obtained by heating form II; (2) form II, transformation product without ultrasound; (3) form V, transformation product in 2-propanol at 308.15 K with 60 W ultrasound; (4) form V + II, transformation product in 1-butanol at 308.15 K with 60 W ultrasound.

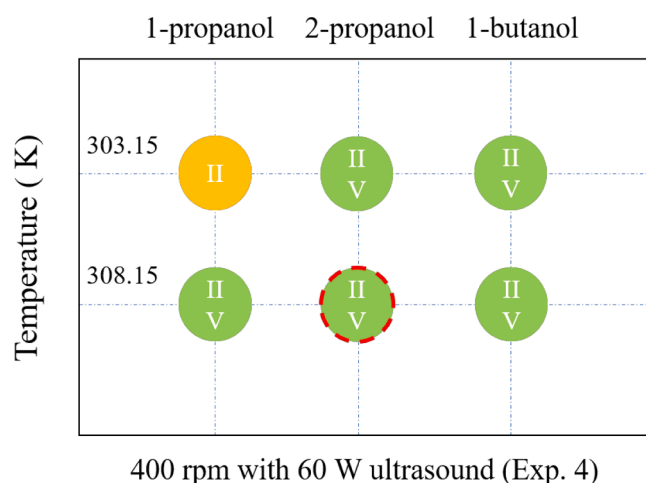


Fig. 6. The summary of polymorphs collected from the reconstruction zone in the solvent-mediated transformation process. (Yellow solid circle: pure form II; Green solid circle: form II and form V, Red dotted line surrounding green solid circle: amounts of form V with trace form II). (For interpretation of the references to colour in this figure legend, the reader is referred to the web version of this article.)

nucleated after the induction period in 1-propanol at 303.15 K, while both form II and form V crystals were nucleated in 2-propanol and 1-butanol at the same transformation temperature. At 308.15 K, the concomitant nucleation of form II and form V occurred in all of the solvents (Fig. S8(b)). Especially in 2-propanol, amounts of form V crystals with trace form II crystals were nucleated after the induction period (the insert image in Fig. S8(b)). Thus, the higher temperature might be more favorable to the nucleation of form V crystals.

Many studies have reported that the ultrasound could selectively promote the appearance of one polymorph in solution crystallization [25,57,58]. Based on the stability experiments, form V was identified as a metastable polymorph, which was less stable than form II. From the thermodynamics point of view (shown in Fig. S9), the ultrasound could provide enough energy to overcome the critical energetic barrier for nucleation, and eventually promote spontaneous nucleation [54] of form V. From the dynamics point of view, the ultrasound could increase the local high supersaturation which tends to the nucleation of the metastable form, and consequently increases the nucleation rate of the metastable form [53]. When the nucleation rates of the metastable and stable forms were almost the same, the concomitant nucleation would occur.

Therefore, in this study, ultrasound-assisted nucleation provided an alternative approach to produce theophylline form V. The existing approaches in the literature include the supercritical antisolvent precipitation [30] and crystallization in methanol [35]. In addition, significant amounts of form V could be produced, which allows the use of traditional PXRD to detect this form and overcomes the detected limitations due to the low yield proposed in the literature [35]. The high repeatability and the diversity of available solvents (1-propanol, 2-propanol and 1-butanol) made the elusive form V easier to produce.

3.3.2. Connection between the ultrasound-promoted efficiency of nucleation and solute-solvent interaction

Solute-solvent interactions were probed by DFT calculations using a Gaussian 09 package [59]. The details were described in the Supporting Information. In this system, the alcoholic molecules expressed both H-bond donor capability and H-bond acceptor capability, which could respectively form strong H-bonds with H-bonds acceptor sites and H-bonds donor sites of theophylline. The electrostatic potential map (EPM) of theophylline was depicted in Fig. S10 (plotted by *Multivfn* and *VMD* [60,61]), which was used for probing (1:1) solute-solvent binding

energies [62]. The electrostatic potential could be applied to analyze the combination strength of a complex mainly assembled by static electricity interaction [60,63], including the hydrogen bond, dihydrogen bond, halogen bond, etc. In general, if the electrostatic potential of an atom in the molecule is more negative (or positive), this atom will show the stronger electrophilic (or nucleophilic) property. Thus, the van der Waals surface EPM of molecules can be applied to predict and select the most active sites which were the main sites for the subsequent calculation of solute–solvent interaction. Three sites with strong electron-rich regions (H-bonds acceptor sites) were selected for calculating solute–solvent binding energies: carbonyl group $C = O$ on the pyrimidine ring (site 1 and site 2) and $C = N_3$ on the asymmetric imidazole ring (site 3). Besides, one site with electron-deficient regions (H-bonds donor site) was also selected for calculating solute–solvent binding energies: N_4-H on the imidazole ring (site 4).

It can be seen from Fig. 7 that the binding energies seem to be the largest at site 1 followed by site 4, site 3 and site 2 in all solvents except 2-propanol. The order of binding energies at site 2 and site 3 in 2-propanol was opposite. Usually, larger binding energy represents a stronger solute–solvent interaction. The solute–solvent binding energies at site 1 increase in the order: 1-propanol (-65.213 kJ/mol) < 1-butanol (-65.427 kJ/mol) < 2-propanol (-65.768 kJ/mol). The order of binding energies at site 2 follows the same order as site 1. However, the order of binding energies at site 3 is different: 2-propanol (-28.473 kJ/mol) < 1-propanol (-32.276 kJ/mol) < 1-butanol (-32.474 kJ/mol), and so does the order at site 4.

The theophylline-solvent heterologous dimers at site 1 consist of the formation of strong $C = O \dots H-O$ hydrogen bond and strong $N-H \dots O-H$ hydrogen bond, resulting in the largest binding energy at site 1. The theophylline-solvent heterologous dimers at site 2 consist of the formation of strong $C = O \dots H-O$ hydrogen bond and weak $C-H \dots O-H$ hydrogen bond. Besides, the unique spatial structure, in which the $C = O$ was located between two methyl groups, increased steric hindrance and hindered the formation of hydrogen bond. Hence, the binding energies at site 2 are the smallest. For the heterologous dimers at site 3, there are strong $O-H \dots N$ hydrogen bond and weak $C-H \dots O-H$ hydrogen bond, and the heterologous dimers at site 4 consist of strong $N-H \dots O-H$ hydrogen and weak $C = O \dots H-C$ hydrogen bond, suggesting that both site 3 and site 4 produce moderate binding energies. The exception of 2-propanol

at site 2 and site 3 may be due to the shape and volume of 2-propanol. The interactions at specific sites between solute molecules and solvent molecules are closely related to the nucleation difficulty of the model compound, which has been identified in many studies: stronger solute–solvent interaction commonly corresponds to be more difficult to nucleate [62,64,65].

As discussed above, without ultrasound, t_{ind} is the largest in 2-propanol, followed by 1-butanol and 1-propanol, which was consistent with the order of binding energies at site 1 and site 2. According to the literatures, if the solution chemistry of a model compound has no direct correlation with its crystal structure, the nucleation period would contain a necessary desolvation process prior to the formation of crystalline clusters [66,67]. The desolvation process continues until the crystalline clusters grow to the critical nuclei to influence the nucleation process [67]. In some crystallization systems, the desolvation process could be the rate-limiting step during the nucleation stage. In general, during the nucleation process, the solvated solute molecules experienced desolvation before the molecules assembled into the cluster surface, which would influence the subsequent nucleation rate in different solvents [68,69]. In brief, the stronger solvation strength would be more difficult for desolvation, corresponding to a lower nucleation rate. The reported studies concerned mostly about the decisive effect of desolvation on the nucleation process in molecular level. Thus, how exactly fast about the desolvation process was not considered in this study. Bobrovs et al. [32] have proved that the theophylline molecules were solvated in methanol, and needed to undergo supramolecular recombination to remove solvent molecules for forming crystal nuclei only containing theophylline molecule structure. Similarly, the FTIR spectra were also applied here to explore the solution chemistry of theophylline molecules in the alcoholic solvents. Fig. S11 showed the solid FTIR spectra of form I, form II and form V. In Fig. S12, the shift of $C = O$ characteristic peaks indicated that solute–solvent complexes were formed in the alcoholic solvents. In other words, the solvation of theophylline molecules also occurred in 1-propanol, 2-propanol and 1-butanol. Except for the solution chemistry, the crystal structure of form II was considered next. The hydrogen bonding pattern of theophylline form II was clearly expressed in Fig. S13. The strongest hydrogen bond donor (N_4-H) on one molecule bonds to the strong hydrogen bond acceptor ($C = N_3$) on the adjacent molecule, forming an $R_2^2(8)$ motif.

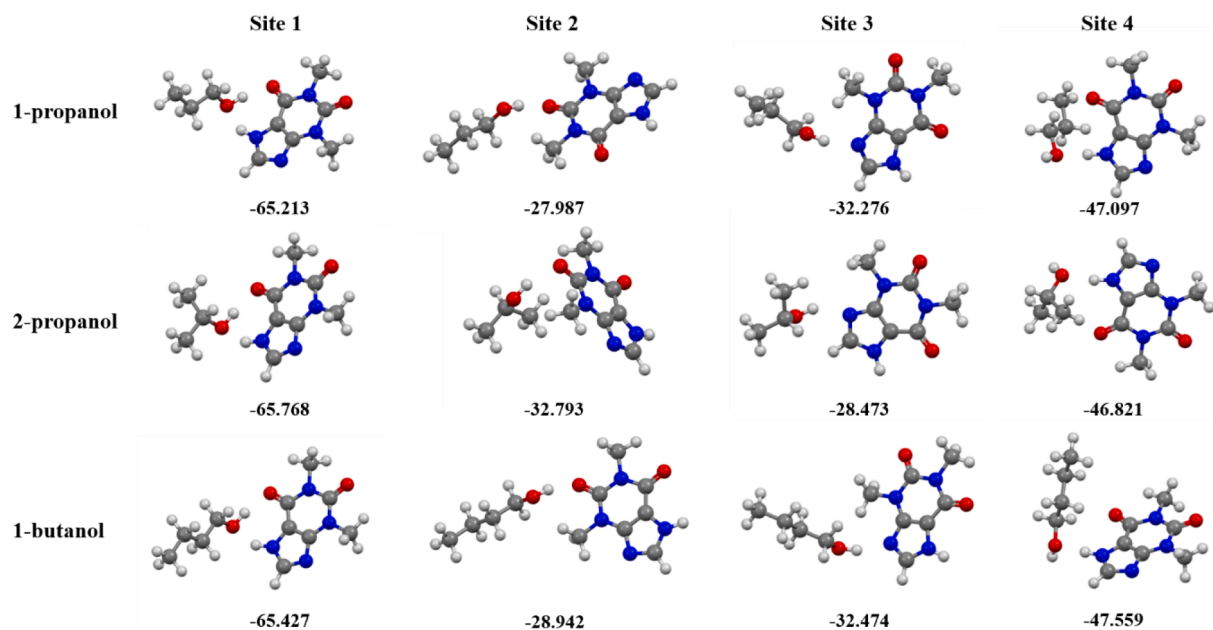


Fig. 7. Optimized geometries and binding energies (kJ/mol) for 1:1 theophylline-solvent complexes, calculated at B97d3/6-31G (d, p) level. Carbon-grey, hydrogen-white, oxygen-red, nitrogen-blue. (For interpretation of the references to colour in this figure legend, the reader is referred to the web version of this article.)

Thus, the solution chemistry of theophylline was significantly different with the crystal structure of theophylline form II. As a result, the complete desolvation of solute molecules is the rate-limiting step before the nucleation of target crystals. Thus, the solute–solvent interaction at site 1, having the largest binding energy, seemed to determine the nucleation rate in the case without the ultrasound.

As mentioned above, the nucleation-promoted efficiencies by ultrasound at 303.15 K followed the order of 1-propanol < 1-butanol < 2-propanol. At 303.15 K, the concomitant nucleation of metastable form V and stable form II crystals occurred in 2-propanol and 1-butanol, with pure form II nucleated in 1-propanol. In the concomitant nucleation, the high nucleation rate was affected by the combination of thermodynamic and kinetic factors, which was larger than the nucleation rate of the stable crystals that was only affected by thermodynamic factor [70,71]. It indicated that the ultrasound had a larger effect on the nucleation process in 2-propanol and 1-butanol. Therefore, the nucleation-promoted efficiencies in these two solvents were improved significantly compared to the promoted efficiencies in 1-propanol. For the situation with concomitant nucleation of form II and form V, the nucleation-promoted efficiency by ultrasound was in the order of 1-butanol < 2-propanol at 303.15 K, and 1-butanol < 1-propanol < 2-propanol at 308.15 K. The order was consistent with that of nucleation difficulty reflected by binding energies at site 3 and site 4: the easiest in 2-propanol followed by 1-propanol and 1-butanol. The mechanisms behind the ultrasound-assisted nucleation were explained in this study, by combining the evaporation hypothesis [53,72] and segregation hypothesis [73,74]. A certain amount of solvent would be vaporized during the growth of cavitation bubbles forming local supersaturation at the bubble wall. When the cavitation bubbles begin to collapse, the solvated solute molecules and clusters are segregated from the solvent molecules by the influence of huge pressure gradients (induced by cavitation bubbles) during a very short period of time [75]. The denser species (solvated solute molecules and clusters) will aggregate near the bubble wall producing supersaturation. Both of these two mechanisms illustrated that amounts of solvated solute molecules were concentrated around the cavitation bubbles, and the molecular collision was intensified by ultrasound. Therefore, there was no time to wait for the complete desolvation of the site with the strongest solute–solvent interaction

(site 1) to form clusters. Then, the solvated clusters were generated by the sites (site 3 and 4) having lower binding energy during supramolecular recombination. In the presence of ultrasound, the binding energies at site 3 and site 4 (the sites linked to be the chain motif in the crystal structure), seemed to be more predominant in the nucleation process. In Table 3, the t_{ind} with 60 W ultrasound (Exp. 4) in 2-propanol was far smaller than that in 1-butanol and almost the same as that in 1-propanol. While, t_{ind} in 2-propanol was the largest without ultrasound. The experimental results demonstrated again that the interaction site affecting the nucleation rate gradually changed from site 1 to site 3 and site 4. In the presence of ultrasound, the site with the strongest interaction (site 1) no longer determined the order of nucleation rate, and the sites with weaker interaction (site 3 and site 4) seemed to be more predominant in the nucleation process. In brief, it could be inferred that the ultrasound might change and magnify the decisive effect of specific site on the nucleation rate, under the premise that the ultrasound facilitated the desolvation of all the four sites.

3.3.3. Molecular self-assembly nucleation mechanism affected by ultrasound

Fig. 8 presented the production of cavitation bubbles and the possible molecular self-assembly nucleation pathway which might occur during the collapse of cavitation bubbles. An incomplete desolvation process prior to the formation of chain motif, existed in the nucleation process during the polymorphic transformation. The effect of ultrasonic irradiation on the nucleation process could be mainly attributed to the cavitation effect and microstreaming [76,77]. Based on the cavitation effect, many hypotheses explaining the nucleation process affected by ultrasound were proposed [53,72,78], such as the cooling hypothesis, pressure hypothesis, evaporation hypothesis, segregation hypothesis, etc. These hypotheses indicated that the formation and collapse of the cavitation bubbles could bring high local supersaturation around the cavitation bubbles and intensify the molecular effective collision, promoting the nucleation process [53,54]. With ultrasound, high local supersaturation was achieved by cavitation effect, and more solute–solvent complex molecules did not have enough time to completely remove the solvent molecules in the desolvation process, and directly led to the supramolecular recombination to form solvated

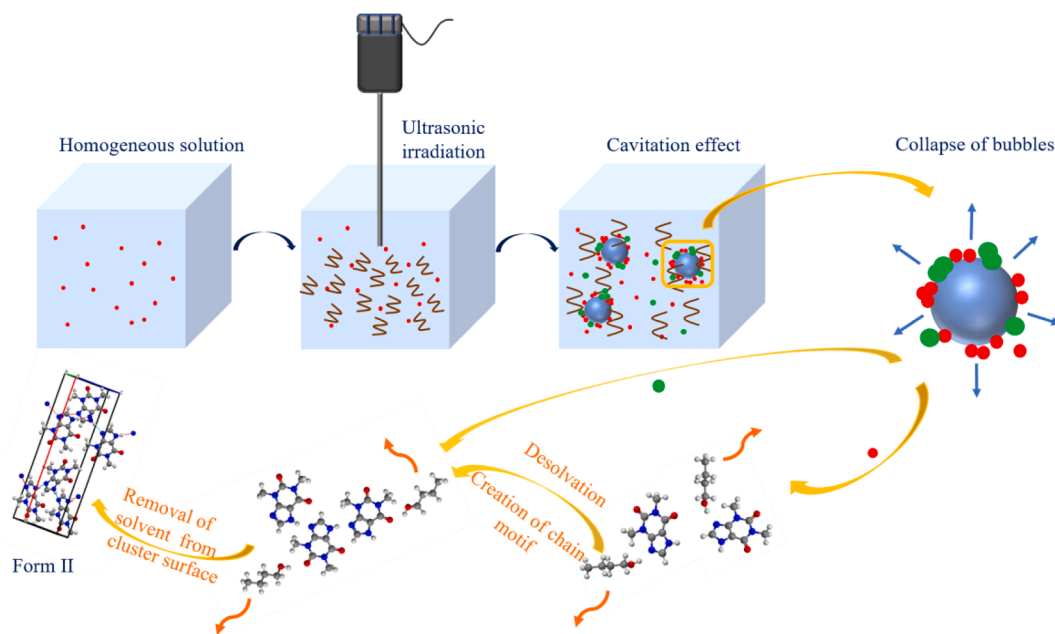


Fig. 8. The proposed schematic diagram of nucleation mechanism in the polymorphic transformation process affected by ultrasound. (Blue solid balls, red solid circles and green solid circles represent for cavitation bubbles, solvated solute molecules and solvated clusters, respectively). (For interpretation of the references to colour in this figure legend, the reader is referred to the web version of this article.)

theophylline clusters. Then, the solvated clusters would undergo desolvation again to form nuclei with theophylline-theophylline structure, and finally grew into larger crystals. Although the ultrasound promoted the desolvation of all the sites, the decisive effect of site 3 and site 4 on the nucleation rate was highlighted due to the weaker solute-solvent interaction of these two sites. The sites 3 and 4 recombined chain motif and would gradually become the rate-limiting step to form critical nuclei in the presence of ultrasound. The rate-limiting step of nucleation in the transformation process was no longer determined by the binding energy at site 1 merely.

Besides, in Table 3, the orders of growth-promoted efficiency were also consistent with the orders of nucleation-promoted efficiency at respective temperatures (303.15 K and 308.15 K). It seems that the ultrasound also influenced the growth rate of product crystals in the transformation process. But because more than one polymorph (form II and form V) was nucleated in the polymorphic transformation, the transformation of form V to form II was also included in the reconstruction zone. Therefore, it is too difficult to analyze how the ultrasound influenced the reconstruction zone from the molecular perspective, let alone the whole transformation process.

3.4. Effect of ultrasound on transformation kinetics

3.4.1. Fitting of transformation kinetic parameters

In 1-propanol at 303.15 K, the pure theophylline form II crystals were obtained in the presence and absence of ultrasonic irradiation (Exp. 1 - Exp. 4), as shown in the PXRD patterns in Fig. S14. The changes of transformation kinetics with ultrasonic modes were discussed in 1-propanol. In each ultrasonic mode, six samples were collected to determine the change of polymorph composition. In Fig. S14, the characteristic peaks located at 7.1° and 12.6° were tracked for monitoring the solid content change of form II, and the characteristic peak located at 11.2° was used to track form I. In the induction zone of the transformation process, only form I crystals existed in the solution. Then, the characteristic peak intensity of form I decreased gradually, and the characteristic peak intensity of form II increased over time. After the reconstruction zone, the characteristic peak of form I disappeared with form II remained at constant peak intensity, which indicated that the transformation process completed. The results monitored by PXRD had good consistency with those obtained by on-line Raman (Fig. 3).

Due to the different characteristic peaks of form I and form II, the polymorphic fractions were calculated by the peaks at 7.1° and 11.2° , which could be used to analyze the kinetics of transformation process. The detailed method for quantitative analysis of phase transformation has been reported and applied in many transformation systems [26,79]. The Avrami-Erofeev model which could describe the thermally activated solid state processes including nucleation and nuclei growth, was usually applied to detect polymorphic transformation process [80,44]. The mathematical expression of Avrami-Erofeev model is listed in Eq. (2) [80]. X represents the mass fraction of theophylline at corresponding transformation time (t). The k and n stand for the rate constant and Avrami exponent, which are obtained by fitting the experimental data with Avrami-Erofeev model (Eq. (2)).

$$X = 1 - \exp[-(k \times t)^n] \quad (2)$$

Fig. 9 described that the mass fractions of theophylline form I and form II change with transformation time, in the absence and presence of ultrasound (Exp.1-4), illuminating the variation trend of transformation kinetics along with varying effective ultrasonic energies. The fitting parameters were listed in Table S1. The total transformation time with 60 W ultrasound (Exp. 4, 150 min) had a sharp decline compared to that without ultrasound (Exp. 1, 576 min). Although the ultrasound could decrease the nucleation induction time of form II (240-60 min), the induction time was always present during the transformation process (Exp.1 to Exp. 4) and accounted for almost 40% of the total transformation time. It seemed that the competitive relationship among

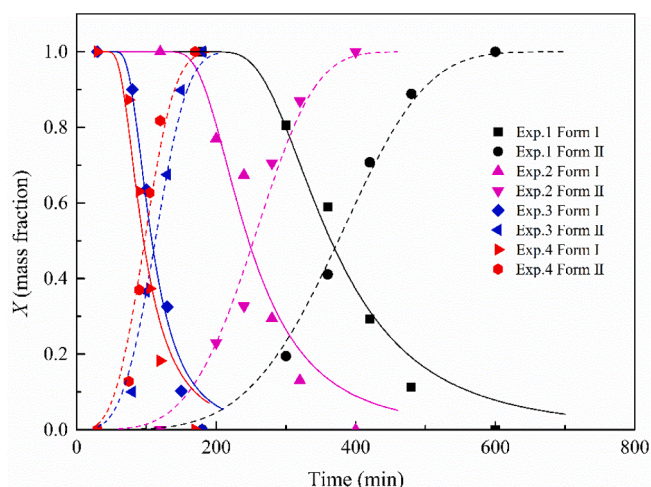


Fig. 9. Plots of transformation kinetics analysis with different effective ultrasonic energies: Exp. 1 - Exp. 4.

dissolution of metastable form, nucleation of stable form and the growth of stable form changed a little, in the presence or absence of ultrasonic irradiation. In other words, the rate-limiting steps in the transformation process within these four experiments might be similar.

3.4.2. Variation of transformation kinetics

To further analyze the transformation kinetics quantitatively, the model parameters k and n were analyzed and depicted in Fig. 10. k represented the transformation rate and n reflected the crystallization mechanism during the transformation process.

In Fig. 10, the Avrami exponent n decreased slowly, and the rate constant k increased slowly, though with stronger ultrasonic energy input (Exp. 1 to Exp. 4). In Exp. 2 (6 W, 11.76% duty cycle), the value of n remained at 4, which was nearly the same as that without ultrasound (Exp. 1). Then in Exp. 3, keeping the same ultrasonic power and increasing the duty cycle (50%), which increased the ultrasonic energy per unit time, the value of n declined to 3. In Exp. 4, maintaining the same duty cycle as that in Exp. 3 and making a significant increase in ultrasonic power (60 W), the value of n still remained at 3. It could be inferred that the Avrami exponent n was not strongly dependent on the ultrasonic power. Similar results were also obtained for the variation tendency of k . The order of magnitude for k was always 10^{-3} in the absence of ultrasonic irradiation (Exp. 1) compared to the case with the

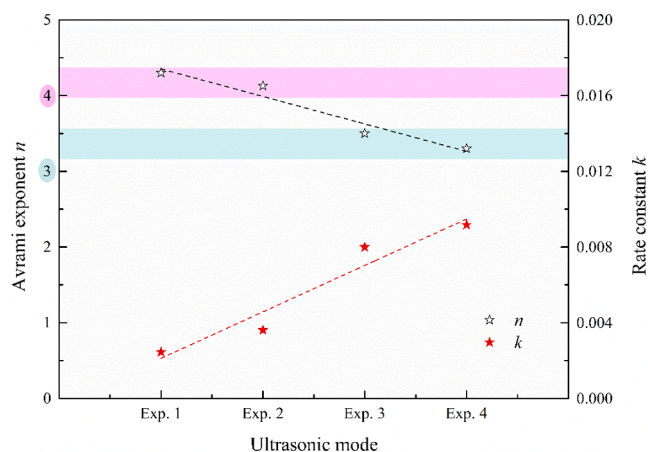


Fig. 10. Avrami-Erofeev model parameters k and n change with different effective ultrasonic energies (Exp. 1 - Exp. 4). The dashed lines represent the tendency of the data points.

strongest ultrasonic energy (Exp. 4). The increase of k could be attributed to the decrease of nucleation period and reconstruction period. But the decreases of two periods were nearly equal proportions, which indirectly reflected that the transformation mechanism did not change obviously. While, in the case of the polymorphic transformation system of L-glutamic acid in water, the induction period disappeared with the application of 27 W ultrasound, and the transformation rate-limiting step changed from the nucleation-growth to the growth [26]. Therefore, the value of k in the L-glutamic acid transformation system (from 0.00235 to 0.0238) [26] was much higher than that in the theophylline transformation system in this study (from 0.00245 to 0.00917).

In the polymorphic transformation kinetics, $n = 3$ represents three-dimensional growth of nuclei [44,81]. $n = 4$ is considered as three-dimensional growth with a constant nucleation rate, in which the constant nucleation rate can be regarded as a growth dimension [82]. Nishida et al. verified that the Avrami exponent n was not the unique parameter to characterize transformation kinetics [83]. Thus, to describe the transformation kinetics more clearly, the analysis should be combined with specific circumstance (described in Fig. 3) in a given transformation system. As discussed in Fig. 3(a), although the nucleation of stable form was the rate-limiting step, the effect of dissolution and growth could not be neglected. Because the morphology of theophylline form II was thin flakes (Fig. S4), the nuclei growth of theophylline form II was assumed to be two-dimensional. Then, it could be inferred that $n = 4$ represented a constant nucleation rate of form II, a two-dimensional growth of form II, and a dissolution rate of form I. In the presence of ultrasound (Exp. 3 and Exp. 4), the dissolution rate of form I became larger than the growth rate of form II, and the nucleation-growth process gradually became the rate-limiting step (Fig. 3(c) and (d)). Then, $n = 3$ corresponded to a constant nucleation rate and a two-dimensional growth of nuclei. The transformation kinetics results matched well with the rate-limiting step obtained by the relationship between solid content and solution concentration. In consequence, there is no need to further increase the ultrasonic energy for changing the transformation kinetics in this system.

4. Conclusion

The solvent-mediated polymorphic transformation of theophylline with the application of ultrasound was explored in three alcoholic solvents (1-propanol, 2-propanol and 1-butanol). The total transformation time (t_{total}) was divided into two parts for detail analysis: the induction period (t_{ind}) and reconstruction period (t_r) of the stable form, which was significantly decreased by ultrasound. The ultrasonic irradiation enhanced the transformation rate, about 1.6–7.6 times compared to that without ultrasound. Three sites with strong electron-rich regions (site 1–3) and one site with electron-deficient regions (site 4) on the theophylline molecule were selected to be H-bonds acceptor site and H-bonds donor site, respectively, for discussing the intensity of solute–solvent interaction. Based on the DFT calculation, the binding energies of 1:1 solute–solvent complexes were calculated for studying the effect of ultrasound on solute–solvent interactions. In different alcoholic solvents, the binding energies were the largest at site 1 (~65 kJ/mol), followed by site 4 (~47 kJ/mol), site 3 (~32 kJ/mol) and site 2 (~28 kJ/mol). Without ultrasound, the t_{ind} followed the order of 1-propanol < 1-butanol < 2-propanol, which was consistent with the order of binding energies at site 1. This indicated that the solute–solvent interaction at site 1 determined the nucleation rate in the absence of ultrasonic irradiation. While, with the application of ultrasound (60 W), the order of t_{ind} changed to 1-propanol \approx 2-propanol < 1-butanol, which corresponded to the weakest binding energies in 2-propanol at site 3 and site 4. It seemed that the solute–solvent interaction at site 3 and site 4 began to play a more significant role in determining the nucleation rate, under the influence of ultrasound. The ultrasound-promoted efficiencies of nucleation followed the order of 1-butanol < 1-propanol < 2-propanol, which was consistent with the order of nucleation difficulty

reflected by binding energies at site 3 and site 4: the easiest in 2-propanol followed by 1-propanol and 1-butanol. Consequently, in the system need to experience desolvation before nucleation, the ultrasound might influence the solute–solvent interaction site that determined the nucleation rate.

In addition, the variation of transformation rate-limiting step in the presence of ultrasound was preliminarily estimated by the real-time relative change of solid-state composition and solution concentration. The Avrami-Erofeev model was used to fit the transformation kinetic parameters k and n . The rate-limiting step changed from the nucleation dominated with equal dissolution rate and growth rate ($n \approx 4$, without ultrasound) to the nucleation-growth dominated ($n \approx 3$, 60 W ultrasound). It is worth mentioning that the elusive theophylline form V was produced in the polymorphic transformation with ultrasound, for the first time, in the present study. The highly pure form V crystals (with trace amounts of form II) could be produced in 2-propanol with repeatable and steady operation.

CRedit authorship contribution statement

Chen Fang: Investigation, Writing – original draft, Data curation, Formal analysis. **Peng Yang:** Conceptualization, Validation. **Yumin Liu:** Formal analysis. **Jingkang Wang:** Funding acquisition, Project administration. **Zhenguo Gao:** Supervision. **Junbo Gong:** Funding acquisition, Project administration. **Sohrab Rohani:** Writing - review & editing.

Declaration of Competing Interest

The authors declare that they have no known competing financial interests or personal relationships that could have appeared to influence the work reported in this paper.

Acknowledgments

The authors are grateful to the financial support of the National Natural Science Foundation of China (NOS. NNSFC 21808159, 22008173 and 21676179), the National Key Research and Development Program of China (No. 2020BZ-0005), the open foundation of the State Key Laboratory of Chemical Engineering (NO. SKL-ChE-18B04), and Major National Science and Technology Projects 2017ZX09101001.

References

- [1] R. Purohit, P. Venugopalan, Polymorphism: an overview, *Resonance* 14 (2009) 882–893.
- [2] A. Llinàs, J.M. Goodman, Polymorph control: past, present and future, *Drug Discov. Today* 13 (5–6) (2008) 198–210.
- [3] T. Zhang, B. Szilágyi, J. Gong, Z.K. Nagy, Thermodynamic polymorph selection in enantiotropic systems using supersaturation-controlled batch and semibatch cooling crystallization, *Cryst. Growth Des.* 19 (11) (2019) 6715–6726.
- [4] W. Ostwald, Studien über die Bildung und Umwandlung fester Körper. 1. Abhandlung: Übersättigung und Überkaltung, *Z. Phys. Chem.* 22 (1897) 289–330.
- [5] W. Tang, A.D. Sima, J. Gong, J. Wang, T. Li, Kinetic difference between concomitant polymorphism and solvent-mediated phase transformation: a case of tolfenamic acid, *Cryst. Growth Des.* 20 (3) (2020) 1779–1788.
- [6] C. Chen, O. Cook, C.E. Nicholson, S.J. Cooper, Leapfrogging Ostwald's rule of stages: crystallization of stable γ -glycine directly from microemulsions, *Cryst. Growth Des.* 11 (2011) 2228–2237.
- [7] C.H. Gu, V. Young Jr., D.J.W. Grant, Polymorph screening: influence of solvents on the rate of solvent-mediated polymorphic transformation, *J. Pharm. Sci.* 90 (2001) 1878–1890.
- [8] S. Lee, A. Choi, W.-S. Kim, A.S. Myerson, Phase transformation of sulfamerazine using a Taylor vortex, *Cryst. Growth Des.* 11 (11) (2011) 5019–5029.
- [9] C. Stoica, P. Tinnemans, H. Meeke, E. Vlieg, Epitaxial 2D nucleation of metastable polymorphs: a 2D version of Ostwald's rule of stages, *Cryst. Growth Des.* 5 (2005) 975–981.
- [10] T.D. Turner, S. Caddick, R.B. Hammond, K.J. Roberts, X. Lai, Kinetics of the aqueous-ethanol solution mediated transformation between the beta and alpha polymorphs of p-aminobenzoic acid, *Cryst. Growth Des.* 18 (2) (2018) 1117–1125.

- [11] H.-J. Kim, K.-J. Kim, In situ monitoring of polymorph transformation of clopidogrel hydrogen sulfate using measurement of ultrasonic velocity, *J. Pharm. Sci.* 97 (10) (2008) 4473–4484.
- [12] J. Cornel, C. Lindenberg, M. Mazzotti, Experimental characterization and population balance modeling of the polymorph transformation of L-glutamic acid, *Cryst. Growth Des.* 9 (2009) 243–252.
- [13] R.J. Davey, N. Blagden, S. Righini, H. Alison, E.S. Ferrari, Nucleation control in solution mediated polymorphic phase transformations: the case of 2,6-dihydroxybenzoic acid, *J. Phys. Chem. B* 106 (2002) 1954–1959.
- [14] W. Du, Q. Yin, J. Gong, Y. Bao, X. Zhang, X. Sun, S. Ding, C. Xie, M. Zhang, H. Hao, Effects of solvent on polymorph formation and nucleation of prasugrel hydrochloride, *Cryst. Growth Des.* 14 (9) (2014) 4519–4525.
- [15] A. Maher, D.M. Croker, C.C. Seaton, Å.C. Rasmuson, B.K. Hodnett, Solution-mediated polymorphic transformation: form II to form III piracetam in organic solvents, *Cryst. Growth Des.* 14 (2014) 3967–3974.
- [16] M. Kurotani, I. Hirasawa, Polymorph control of sulfamerazine by ultrasonic irradiation, *J. Cryst. Growth* 310 (21) (2008) 4576–4580.
- [17] M. Kurotani, I. Hirasawa, Effect of ultrasonic irradiation on the selective polymorph control in sulfamerazine, *Chem. Eng. Res. Des.* 88 (9) (2010) 1272–1278.
- [18] R. Bobrovs, L. Seton, A. Actiņš, Solvent-mediated phase transformation between two tefagur polymorphs in several solvents, *CrystEngComm*. 16 (46) (2014) 10581–10591.
- [19] S. Wu, M. Chen, S. Rohani, D. Zhang, S. Du, S. Xu, W. Dong, J. Gong, Solvent-mediated nonoriented self-aggregation transformation: a case study of gabapentin, *Cryst. Growth Des.* 17 (8) (2017) 4207–4216.
- [20] Z. Guo, A.G. Jones, N. Li, The effect of ultrasound on the homogeneous nucleation of BaSO₄ during reactive crystallization, *Chem. Eng. Sci.* 61 (2006) 1617–1626.
- [21] T. Hazi Mastan, M. Lenka, D. Sarkar, Nucleation kinetics from metastable zone widths for sonocrystallization of L-phenylalanine, *Ultrason. Sonochem.* 36 (2017) 497–506.
- [22] Z.Y. Ma, A.M. Pang, W. Li, Y.F. Qi, L.X. Zhang, Preparation and characterization of ultra-fine ammonium perchlorate crystals using a microfluidic system combined with ultrasonication, *Chem. Eng. J.* 405 (2021), 126516.
- [23] A.V. Mohod, P.R. Gogate, Improved crystallization of ammonium sulphate using ultrasound assisted approach with comparison with the conventional approach, *Ultrason. Sonochem.* 41 (2018) 310–318.
- [24] M.N. Hussain, J. Jordens, S. Kuhn, L. Braeken, T. Van Gerven, Ultrasound as a tool for polymorph control and high yield in flow crystallization, *Chem. Eng. J.* 408 (2021) 127272, <https://doi.org/10.1016/j.cej.2020.127272>.
- [25] Y. Mori, M. Maruyama, Y. Takahashi, K. Ikeda, S. Fukukita, H.Y. Yoshikawa, S. Okada, H. Adachi, S. Sugiyama, K. Takano, S. Murakami, H. Matsumura, T. Inoue, M. Yoshimura, Y. Mori, Selective crystallization of metastable phase of acetaminophen by ultrasonic irradiation, *Appl. Phys. Express.* 8 (2015), 065501.
- [26] C. Fang, W. Tang, S. Wu, J. Wang, Z. Gao, J. Gong, Ultrasound-assisted intensified crystallization of L-glutamic acid: crystal nucleation and polymorph transformation, *Ultrason. Sonochem.* 68 (2020) 105227, <https://doi.org/10.1016/j.ultrsonch.2020.105227>.
- [27] R. Prasad, S.V. Dalvi, Sonocrystallization: monitoring and controlling crystallization using ultrasound, *Chem. Eng. Sci.* 226 (2020), 115911.
- [28] S. Piiskop, S. Salmar, A. Tuulmets, A. Kuznetsov, J. Järvi, Kinetic sonication effects in aqueous acetonitrile solutions. Reaction rate levelling by ultrasound, *Ultrason. Sonochem.* 20 (6) (2013) 1414–1418.
- [29] S. Salmar, A. Kuznetsov, A. Tuulmets, J. Järvi, S. Piiskop, Kinetic sonication effects in light of molecular dynamics simulation of the reaction medium, *Ultrason. Sonochem.* 20 (2) (2013) 703–707.
- [30] C. Roy, A. Vegonzalez, P. Subrapatnault, Theophylline formulation by supercritical antisolvents, *Int. J. Pharmaceut.* 343 (1–2) (2007) 79–89.
- [31] D. Khamar, R.G. Pritchard, L.J. Bradshaw, G.A. Hutcheon, L. Seton, Polymorphs of anhydrous theophylline: stable form IV consists of dimer pairs and metastable form I consists of hydrogen-bonded chains, *Acta Cryst. C* 67 (12) (2011) o496–o499.
- [32] R. Bobrovs, L. Seton, N. Dempster, The reluctant polymorph: investigation into the effect of self-association on the solvent mediated phase transformation and nucleation of theophylline, *CrystEngComm*. 17 (2015) 5237–5251.
- [33] M.D. Eddleston, K.E. Hejczyk, A.M.C. Cassidy, H.P.G. Thompson, G.M. Day, W. Jones, Highly unusual triangular crystals of theophylline: the influence of solvent on the growth rates of polar crystal faces, *Cryst. Growth Des.* 15 (2015) 2514–2523.
- [34] K. Fücke, G.J. McIntyre, C. Wilkinson, M. Henry, J.A.K. Howard, J.W. Steed, New insights into an old molecule: interaction energies of theophylline crystal forms, *Cryst. Growth Des.* 12 (2012) 1395–1401.
- [35] M.D. Eddleston, E.G. Bithell, W. Jones, Transmission electron microscopy of pharmaceutical materials, *J. Pharm. Sci.* 99 (9) (2010) 4072–4083.
- [36] X. Li, D. Han, Y. Wang, S. Du, Y. Liu, J. Zhang, B.o. Yu, B. Hou, J. Gong, Measurement of solubility of thiamine hydrochloride hemihydrate in three binary solvents and mixing properties of solutions, *J. Chem. Eng. Data* 61 (10) (2016) 3665–3678.
- [37] J.Y. Ma, X. Huang, N. Wang, X. Li, Y. Bao, T. Wang, H.X. Hao, Solubility and thermodynamic mixing and dissolution properties of empagliflozin in pure and binary solvent systems, *J. Mol. Liq.* 309 (2020), 113004.
- [38] S. Liu, E.G.J. Macarigua, X. Li, L. Jia, Y. Liu, J. Gong, Organic solvent effects on solid-liquid phase equilibrium of D-mannitol and aqueous binary solvents: an experimental and computational study, *J. Mol. Liq.* 238 (2017) 411–422.
- [39] V. Jouyban-Gharamaleki, K. Jouyban-Gharamaleki, J. Soleymani, W.E. Acree, A. Jouyban, Solubility determination of tris(hydroxymethyl)aminomethane in water + methanol mixtures at various temperatures using a laser monitoring technique, *J. Chem. Eng. Data* 59 (7) (2014) 2305–2309.
- [40] J. Lu, S. Rohani, Synthesis and preliminary characterization of sulfamethazine-theophylline co-crystal, *J. Pharm. Sci.* 99 (9) (2010) 4042–4047.
- [41] M. Baranska, L.M. Proniewicz, Raman mapping of caffeine alkaloid, *Vib. Spectrosc.* 48 (1) (2008) 153–157.
- [42] H.G.M. Edwards, T. Munshi, M. Anstis, Raman spectroscopic characterisations and analytical discrimination between caffeine and demethylated analogues of pharmaceutical relevance, *Spectrochim. Acta A* 61 (7) (2005) 1453–1459.
- [43] S. Maruyama, H. Ooshima, Mechanism of the solvent-mediated transformation of taltirelin polymorphs promoted by methanol, *Chem. Eng. J.* 81 (2001) 1–7.
- [44] D.L.T. Nguyen, K.J. Kim, Solvent-mediated polymorphic transformation of a-taltirelin by seeded crystallization, *Chem. Eng. Technol.* 39 (2016) 1281–1288.
- [45] J.-H. An, G.J. Choi, W.-S. Kim, Polymorphic and kinetic investigation of adefovir dipivoxil during phase transformation, *Int. J. Pharm.* 422 (1–2) (2012) 185–193.
- [46] W. Sun, G. Ceder, Induction time of a polymorphic transformation, *CrystEngComm*. 19 (31) (2017) 4576–4585.
- [47] L. Wantha, Kinetics of the solution-mediated polymorphic transformation of organic compounds, *Curr. Pharm. Design* 24 (21) (2018) 2383–2393.
- [48] M.A. O'Mahony, A. Maher, D.M. Croker, Å.C. Rasmuson, B.K. Hodnett, Examining solution and solid state composition for the solution mediated polymorphic transformation of carbamazepine and piracetam, *Cryst. Growth Des.* 12 (4) (2012) 1925–1932.
- [49] S. Thirunahari, P.S. Chow, R.B.H. Tan, Quality by design (QbD)-based crystallization process development or the polymorphic drug tolbutamide, *Cryst. Growth Des.* 11 (2011) 3027–3038.
- [50] Y. Gong, B.M. Collman, S.M. Mehrens, E. Lu, J.M. Miller, A. Blackburn, D.J. W. Grant, Stable-form screening: overcoming trace impurities that inhibit solution-mediated phase transformation to the stable polymorph of sulfamerazine, *J. Pharm. Sci.* 97 (2008) 2130–2144.
- [51] E.S. Ferrari, R.J. Davey, W.I. Cross, A.L. Gillon, C.S. Towler, Crystallization in polymorphic systems: the solution-mediated transformation of β to α glycine, *Cryst. Growth Des.* 3 (2003) 53–60.
- [52] H. Qu, M. Louhi-Kultanen, J. Kallas, Additive effects on the solvent-mediated anhydrate/hydrate phase transformation in a mixed solvent, *Cryst. Growth Des.* 7 (4) (2007) 724–729.
- [53] J. Jordens, B. Gielen, C. Xiouras, M.N. Hussain, G.D. Stefanidis, L.C.J. Thomassen, L. Braeken, T. Van Gerven, Sonocrystallisation: observations, theories and guidelines, *Chem. Eng. Process.* 139 (2019) 130–154.
- [54] S. Nalesso, M.J. Bussemaker, R.P. Sear, M. Hodnett, J. Lee, A review on possible mechanisms of sonocrystallisation in solution, *Ultrason. Sonochem.* 57 (2019) 125–138.
- [55] B.W. Zeiger, K.S. Suslick, Sonofragmentation of molecular crystals, *J. Am. Chem. Soc.* 133 (37) (2011) 14530–14533.
- [56] S. Devarakonda, J.M.B. Evans, A.S. Myerson, Impact of ultrasonic energy on the flow crystallization of dextrose monohydrate, *Cryst. Growth Des.* 4 (4) (2004) 687–690.
- [57] S. Gracin, M. Uusi-Penttilä, Å.C. Rasmuson, Influence of ultrasound on the nucleation of polymorphs of p-aminobenzoic acid, *Cryst. Growth Des.* 5 (5) (2005) 1787–1794.
- [58] S.K. Bhangu, M. Ashokkumar, J. Lee, Ultrasound assisted crystallization of paracetamol: crystal size distribution and polymorph control, *Cryst. Growth Des.* 16 (2016) 1934–1941.
- [59] M.J. Frisch, G.W. Trucks, H.B. Schlegel, G.E. Scuseria, M.A. Robb, J.R. Cheeseman, et al. *Gaussian 09, Revision D.01*; Gaussian Inc., Wallingford, CT, 2013.
- [60] S.Y. Zong, J.K. Wang, H. Wu, Q. Liu, Y.H. Hao, X. Huang, D.H. Wu, G.C. Zhou, H. X. Hao, Insight into the role of pre-assembly and desolvation in crystal nucleation: a case of p-nitrobenzoic acid, *Acta Cryst. B* 75 (2019) 845–854.
- [61] T. Lu, F.W. Chen, Multiwfn: A multifunctional wavefunction analyzer, *J. Comput. Chem.* 33 (2012) 580–592.
- [62] T. Lu, F. Chen, Quantitative analysis of molecular surface based on improved Marching Tetrahedra algorithm, *J. Mol. Graph. Model.* 38 (2012) 314–323.
- [63] M.N. Tahir, M. Khalid, A. Islam, S.M. Ali Mashhadi, A.A.C. Braga, Facile synthesis, single crystal analysis, and computational studies of sulfanilamide derivatives, *J. Mol. Struct.* 1127 (2017) 766–776.
- [64] Y. Chai, L. Wang, Y. Bao, R. Teng, Y. Liu, C. Xie, Investigating the solvent effect on crystal nucleation of etoricoxib, *Cryst. Growth Des.* 19 (3) (2019) 1660–1667.
- [65] M.B. Lynch, S.E. Lawrence, M. Nolan, Predicting nucleation of isonicotinamide from the solvent-solute interactions of isonicotinamide in Common Organic Solvents, *J. Phys. Chem. A* 122 (12) (2018) 3301–3312.
- [66] D. Khamar, J. Zeglinski, D. Mealey, Å.C. Rasmuson, Investigating the role of solvent-solute interaction in crystal nucleation of salicylic acid from organic solvents, *J. Am. Chem. Soc.* 136 (33) (2014) 11664–11673.
- [67] J. Zeglinski, M. Kuhs, K.R. Devi, D. Khamar, A.C. Hegarty, D. Thompson, Å. C. Rasmuson, Probing crystal nucleation of fenoxycarb from solution through the effect of solvent, *Cryst. Growth Des.* 19 (4) (2019) 2037–2049.
- [68] R.A. Sullivan, R.J. Davey, G. Sadiq, G. Dent, K.R. Back, J.H. ter Horst, D. Toroz, R. B. Hammond, Revealing the roles of desolvation and molecular self-assembly in crystal nucleation from solution: benzoic and p-aminobenzoic acids, *Cryst. Growth Des.* 14 (5) (2014) 2689–2696.
- [69] W. Du, L. Bai, Y. Gong, L. Zhang, J. Xiang, S. Wang, N.a. Tang, L. Zhu, Q. Yin, Molecular self-assembly in solution and the nucleation pathway: the case of p-nitrobenzoic acid, *Ind. Eng. Chem. Res.* 58 (51) (2019) 23284–23293.
- [70] L. Jia, Q. Yin, L. Zhou, X. Zhang, C. Wang, W. Du, L. Zhou, Insights into the mechanism of concomitant nucleation of form II and ethanol solvate of spirinolactone in cooling crystallization, *RSC Adv.* 8 (18) (2018) 9697–9706.

- [71] S. Teychené, B. Biscans, Nucleation kinetics of polymorphs: induction period and interfacial energy measurements, *Cryst. Growth Des.* 8 (2008) 1133–1139.
- [72] U.N. Hatkar, P.R. Gogate, Process intensification of anti-solvent crystallization of salicylic acid using ultrasonic irradiations, *Chem. Eng. Process.* 57–58 (2012) 16–24.
- [73] H. Harzali, F. Baillon, O. Louisnard, F. Espitalier, A. Mgaidi, Experimental study of sono-crystallisation of $ZnSO_4 \cdot 7H_2O$, and interpretation by the segregation theory, *Ultrason. Sonochem.* 18 (2011) 1097–1106.
- [74] G. Cravotto, E.C. Gaudino, P. Cintas, On the mechanochemical activation by ultrasound, *Chem. Soc. Rev.* 42 (18) (2013) 7521, <https://doi.org/10.1039/c2cs35456j>.
- [75] J. Dodds, F. Espitalier, O. Louisnard, R. Grossier, R. David, M. Hassoun, F. Baillon, C. Gatamel, N. Lyczko, The effect of ultrasound on crystallisation-precipitation processes: some examples and a new segregation model, *Part. Part. Syst. Charact.* 24 (1) (2007) 18–28.
- [76] A.H. Bari, A. Chawla, A.B. Pandit, Sono-crystallization kinetics of K_2SO_4 : estimation of nucleation, growth, breakage and agglomeration kinetics, *Ultrason. Sonochem.* 35 (2017) 196–203.
- [77] Z.i. Zhang, D.-W. Sun, Z. Zhu, L. Cheng, Enhancement of crystallization processes by power ultrasound: current state-of-the-art and research advances, *Compr. Rev. Food Sci. F.* 14 (4) (2015) 303–316.
- [78] M.D. Luque de Castro, F. Priego-Capote, Ultrasound-assisted crystallization (sonocrystallization), *Ultrason. Sonochem.* 14 (6) (2007) 717–724.
- [79] H.J. Zhu, J. Xu, P. Varlashkin, S. Long, C. Kidd, Dehydration, hydration behavior, and structural analysis of fenoprofen calcium, *J. Pharm. Sci.* 90 (2001) 845–859.
- [80] Y.P. Wang, P.P. Sun, S.J. Xu, S.C. Du, T. Zhang, B. Yu, S.X. Zhang, Y. Wang, Y. W. Wang, J.B. Gong, Solution-mediated phase transformation of argatroban: ternary phase diagram, rate-determining step, and transformation kinetics, *Ind. Eng. Chem. Res.* 56 (2017) 4539–4548.
- [81] P. Cui, Q. Yin, Y. Guo, J. Gong, Polymorphic crystallization and transformation of candesartan cilexetil, *Ind. Eng. Chem. Res.* 51 (39) (2012) 12910–12916.
- [82] E.L. Pang, N.Q. Vo, T. Philippe, P.W. Voorhees, Modeling interface-controlled phase transformation kinetics in thin films, *J. Appl. Phys.* 117 (2015), 175304.
- [83] Y. Nishida, F. Aiga, S. Itoh, Microstructural path analysis of polycrystalline solidification by using multi-phase-field method incorporating a nucleation model, *J. Cryst. Growth* 405 (2014) 110–121.